

Director distortions and singularities in inhomogeneous fieldsNándor Éber,¹ Jana Heuer,^{2,*} Ralf Stannarius,² Gergely Tátrai,^{1,†} and Ágnes Buka¹¹Research Institute for Solid State Physics and Optics, Hungarian Academy of Sciences, P.O. Box 49, H-1525 Budapest, Hungary²Institute of Experimental Physics, Otto-von-Guericke University of Magdeburg, P.O. Box 4120, 39016 Magdeburg, Germany

(Received 21 January 2010; published 5 May 2010)

The effect of the electric-field inhomogeneity has been experimentally studied by polarizing microscopy in a homeotropic nematic liquid crystal in confined electrode geometries which may be relevant in display applications. Defects related to tilt inversion have been detected by monitoring the transmitted intensity profile as a function of the applied voltage. The position of the defects could be controlled by an additional magnetic field breaking the symmetry of the original arrangement. The phenomenon has been interpreted via numerical calculation of the director distribution using the continuum theory of nematics. The influence of oblique light incidence and of weak anchoring has also been analyzed. Simulations have provided good qualitative agreement with the observations. The method has turned out to be a sensitive tool to detect small misalignment angles between the magnetic field and the cell plane.

DOI: [10.1103/PhysRevE.81.051702](https://doi.org/10.1103/PhysRevE.81.051702)

PACS number(s): 61.30.Gd, 61.30.Dk, 61.30.Jf

I. INTRODUCTION

A specific feature of nematic liquid crystals is manifested in the coupling between their director \mathbf{n} and the external electric \mathbf{E} and/or magnetic \mathbf{H} fields. Electro- and magneto-optical effects are usually studied in a “sandwich” cell geometry, where the liquid crystal is placed between two parallel transparent solid substrates (x - y plane). The substrates usually are covered with a thin conducting layer in order to be able to apply an electric field across the cell (z direction). The cell thickness d is typically $<100 \mu\text{m}$, while the lateral dimensions D are in the order of cm, which results in a large ($N=D/d > 100$) aspect ratio; hence they can be considered as infinite in the x - y plane. Under such conditions the applied fields are laterally homogeneous, and at proper signs of the anisotropy of the dielectric permittivity or the magnetic susceptibility, fields exceeding a threshold value induce a deformation of the director field homogeneous in x - y , i.e., a deviation from the initial director determined by the surface anchoring [1,2].

Comparison of the director distribution in such “infinite” cells with that in a confined geometry (where the lateral dimensions of the cell or of the electrodes are comparable or just a few times bigger than the thickness, i.e., $N < 10$) is an interesting basic question as well as an important issue in technological applications. In the first case (“infinite” cells) one takes advantage of the large homogeneously deformed area and neglects the boundary effects. This large aspect ratio also makes studying nonequilibrium pattern forming instabilities [3] convenient in this geometry. The second case (small sized cells) has a special importance for the display technology where the lateral size of pixels may be in the range of the thickness or can gain a straightforward application in optics to create liquid crystal microlenses [4,5]. Ear-

lier investigations on the consequences of the inhomogeneous electric field in this confined case have focused on planarly aligned cells [5–8] offering best perspectives for display applications and have reported interesting instabilities of the inversion lines occurring in the center of the pixels [9,10].

On the other hand, several problems in basic research also require small aspect ratio cells. One example is a special type of a nonlinear, pattern forming instability (a transition to a tristable intermittent state in electroconvection) where the effect of the spatial noise in the x - y plane could be isolated by varying the size of the convecting area [11]. Also the system can be guided to specific wave-vector ranges by tuning the cell size in the range of the pattern wavelength [12,13].

Recently the homeotropic alignment began to attract larger attention both for electroconvection studies [14] and for display applications [15]. Therefore in the present paper we address the behavior of homeotropic cells in confined geometries. Experimental results are presented for two-dimensional (2d) (pixel) as well as for one-dimensional (1d) (strip) confinements. We also attempt to give a qualitative explanation of the observed effects supported by numerical simulations using the continuum theory of nematics.

The paper is arranged as follows. In Sec. II we describe the measuring setup and the compound studied. Then the main experimental observations for the 2d confinement are summarized in Sec. III A with a qualitative explanation in Sec. III B. Numerical simulations are first presented for the inhomogeneous electric field in Sec. IV A, followed by discussing the influence of an additional magnetic field in Sec. IV B. The numerical results are compared with experiments in 1d confined geometry in Sec. V A. The effect of an oblique light incidence is discussed in Sec. V B; weak anchoring is addressed in Sec. V C. Finally Sec. VI closes the paper with some conclusions.

II. EXPERIMENTAL SETUP AND MATERIALS

The experiments have been carried out in the confined geometry achieved by a special design of the electrodes. A

*Present address: Hewlett Packard Ltd., Filton Road, Bristol BS34 8QZ, United Kingdom.

†Present address: Tantaki Kft, H-1015 Budapest, Donáti u. 67., Hungary.

glass plate coated with conducting indium-tin-oxide (ITO) layer has been etched to obtain a series of parallel conducting strips whose width D varied in the range of 70–450 μm (comparable with the sample thickness). The conducting strips have been contacted along one side (in a comblike electrode arrangement) in order to be able to apply voltage to all strips simultaneously. Two types of cell configuration (*A* and *B*) have been used. Type *A* cells were assembled in a way that the electrode strips on the glass plates facing each other were running perpendicular. As a result the overlapping electrode strips defined a matrix of rectangular areas (pixels) of various sizes where the liquid crystal is subjected to the electric field. Choosing different areas the behavior of liquid crystals in regions of different aspect ratios $N=D/d$ (≈ 1.5 – 9.5) could be studied. These aspect ratios are much smaller than those typically used in other measurements ($N > 200$). In type *B* cell configuration only one of the glass plates was etched; thus the electrode overlapping defined elongated areas constrained in one direction only. The cells have been driven by a sinusoidal ac voltage U with a frequency of $f=1$ kHz and amplitude of $\sqrt{2}U$.

For the measurements the cell was placed in between two water-cooled Peltier elements having a central hole for optical observations. Heating/cooling of the Peltier elements was controlled by a proportional-integral-differential (PID) controller resulting in a ± 0.1 °C stability of the oven temperature. The hot stage was placed in between the poles of an electromagnet. The magnetic field H could be varied by changing the supply current in the range $\mu_0 H \approx 0$ – 1 T. The sample was illuminated by the nearly monochromatic light of a high intensity light emitting diode (LED). The textures/patterns evolving in the sample have been observed with two crossed polarizers using a long-range microscope Questar Qm100 and recorded by a video camera connected to a frame grabber card. These images have been stored with a spatial resolution of 512×512 and an 8 bit gray scale for further processing.

Commercial nematic mixture Phase 5A (Merck) has been used for the experiments which is almost identical to mixture Phase 5 (Merck) except that it contains a dopant added in order to enhance conductivity and promote homeotropic alignment. The compound has negative dielectric permittivity anisotropy ($\epsilon_a < 0$) and positive diamagnetic susceptibility anisotropy ($\chi_a > 0$); other parameters of the substance are also known [16]. Homeotropically aligned sandwich cells of thickness $d=47 \pm 0.4$ μm have been prepared with lateral dimensions of 1 cm \times 1 cm in the x - y plane. As Phase 5A spontaneously aligns homeotropically on clean surfaces, no substrate coating was needed to obtain good orientation. Electric field (\mathbf{E}) has been applied along z and magnetic field (\mathbf{H}) along x .

In this geometry a bend Freedericksz transition (a director tilt homogeneous in x - y) can be induced either by an applied voltage exceeding the threshold voltage U_F or by a magnetic field above the threshold H_F . For the bulk electric and magnetic Freedericksz thresholds $U_F=7.97$ V and $\mu_0 H_F=0.187$ T have been found, respectively. From now on all voltages and magnetic fields will be measured in units of U_F and H_F , respectively. If electric and magnetic fields are superposed the bulk Freedericksz transition occurs at lower

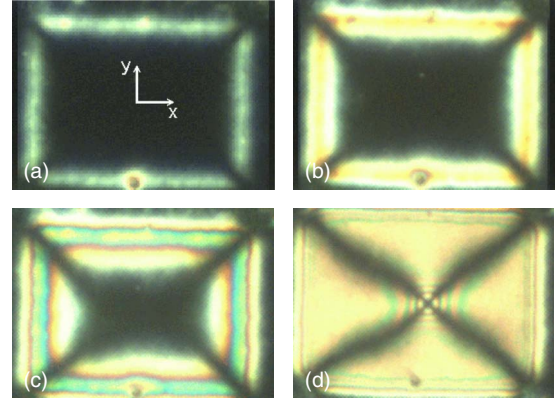


FIG. 1. (Color online) Snapshots taken at crossed polarizers demonstrating the electric-field induced pattern in a rectangular pixel of low aspect ratio (type *A* cell). The applied voltages are (a) $U=0.83U_F$, (b) $U=0.95U_F$, (c) $U=1.03U_F$, and (d) $U=1.17U_F$, respectively.

voltages and fields; for a given $U < U_F$ the threshold magnetic field becomes $H_{UF}=H_F(1-U^2/U_F^2)^{1/2}$ [2].

III. RECTANGULAR (2D) CONFINEMENT

A. Experimental observations on type *A* cells

First we present our observations on type *A* cells representing a two-dimensional rectangular confinement (pixel). At zero applied voltage, $U=0$, the cell has a homogeneous homeotropic orientation; the locations of the overlapping electrodes cannot optically be identified. The effect of the constrained geometry becomes apparent when a voltage is applied to the cell. Figures 1(a)–1(d) exhibit a sequence of images of a pixel of $410 \mu\text{m} \times 410 \mu\text{m}$ taken with crossed polarizers at various U . It is seen that a distortion of the director field manifested in colored bright stripes appearing due to the birefringence variations emerges [see Fig. 1(a)] along the contours of the electrodes already at voltages much below the bulk Freedericksz threshold U_F . For increasing voltages it penetrates gradually into the overlapped electrode region (symmetrically from all four sides) while for $U > U_F$ the distortion extends over the whole region but its very center which remains undistorted as a singular inversion line running normal to the substrates [seen as a black spot in Fig. 1(d)]. At further increase in U one can reach the critical voltage U_c for the onset of electroconvection ($U_c \approx 16.5$ V for $f=1000$ Hz). The appearing electroconvection pattern is characterized by a sequence of dark and bright stripes running normal to the local director (normal rolls) as shown in Figs. 2(a) and 2(b) which, however, preserves the fourfold symmetry of the underlying Freedericksz state [Fig. 1(d)].

When an additional magnetic field \mathbf{H} is applied along one electrode strip (x), the fourfold symmetry of the Freedericksz state seen in Fig. 1 is broken. It is found that the singular inversion line in the center of the cell transforms into an inversion wall in the y - z plane perpendicular to \mathbf{H} as seen in Figs. 3(a)–3(c). One can also notice that this wall shifts to the right with increasing H . The H dependence of the dis-

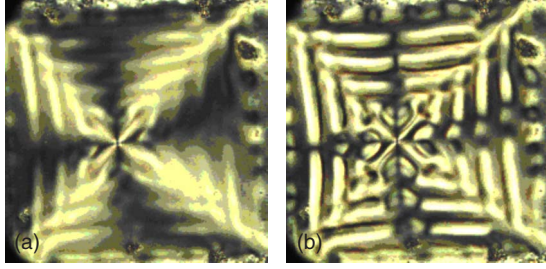


FIG. 2. (Color online) Electroconvection patterns in confined geometry (a) around the threshold voltage U_c and (b) above U_c .

placement s from the center is depicted in more detail in Fig. 4 at a fixed applied voltage of $U=0.8U_F$.

B. Qualitative interpretation

The starting point for the qualitative interpretation of the observations above is the fact that in our cell construction the linear extensions D of a pixel are comparable to the cell thickness d . It is well known from the electrostatics of a plane condenser that around its edges an inhomogeneous electric field develops whose direction and magnitude vary with the distance from the edge. These considerations can readily be applied here with the complication that—in contrast to vacuum or to simple dielectric materials with a constant permittivity—there is an interaction here between \mathbf{E} and the director \mathbf{n} . This results in a director realignment which influences the effective dielectric permittivity and hence \mathbf{E} .

In the region of the inhomogeneous field, where \mathbf{E} acquires a lateral (x or y) component, the dielectric torque induces a tilt of the director, i.e., distortion takes place already for $U < U_F$. One expects that the electrode normal (\mathbf{z}), the director and the electric field are coplanar (Fig. 5), consequently the liquid crystal suffers a 2d splay-bend deformation. The resulting birefringence leads to the intensity modulation seen in Figs. 1(a)–1(d). In Sec. IV A we will calculate numerically the director field induced by the inhomogeneous \mathbf{E} in the plane normal to the electrode edge. As circling along the contour of the overlapping electrode area the lateral component of \mathbf{E} makes a full turn. The direction of the director tilt should also turn around; this is manifested in the fourfold symmetry and in the singularity seen in the center in Fig. 1(d).

Switching on a magnetic field \mathbf{H} along one electrode strip (x) breaks the degeneracy of the homeotropic alignment; due

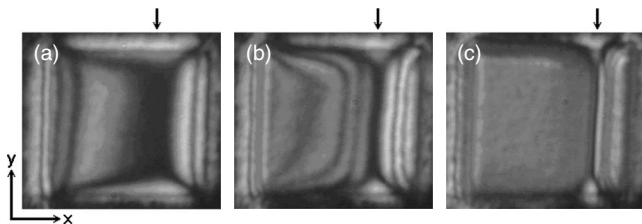


FIG. 3. Snapshots of the field induced patterns in confined geometry at superimposed electric and magnetic fields in a type A cell at $U=0.8U_F$. The arrows indicate the location of the inversion wall. The magnetic fields are (a) $H=0.71H_F$, (b) $H=0.81H_F$, and (c) $H=0.93H_F$, respectively.

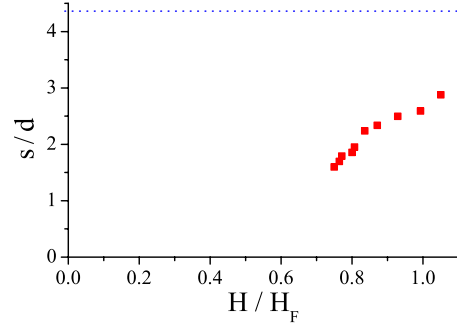


FIG. 4. (Color online) Shift s of the defect wall from the center (in units of the sample thickness d) versus the magnetic field H (in units of the Fredericksz field H_F) at $U=0.8U_F$ in a type A cell. The dotted line marks the location of the electrode edge.

to $\chi_a > 0$ it introduces a preferred direction parallel to \mathbf{H} for the director in the plane of the cell surface (x - y plane). Therefore the electrode edges along x and along y are not equivalent any more which breaks the fourfold symmetry.

For the edge running in the y direction, \mathbf{E} and \mathbf{H} are still coplanar with \mathbf{z} , hence a plane deformation is expected; however, this does not hold for the edge along x where a more general 3d director distortion is anticipated. As director tilts perpendicular to \mathbf{H} are less favored, it is not surprising that the system minimizes the size of that area; i.e., the inversion line extends into an inversion wall along y . If \mathbf{H} is exactly along x , a twofold right/left symmetry of the cell still should prevail; hence the defect wall should be located in the center. This symmetry breaks if the magnetic field is oblique, i.e., if $H_z \neq 0$. The shift of the defect wall to one side in the experiment [as seen in Fig. 3(c)] indicates that there was a misalignment of the magnetic field direction. In Sec. IV B we calculate numerically the influence of \mathbf{H} on the director field and will estimate the misalignment angle occurred during the experiment.

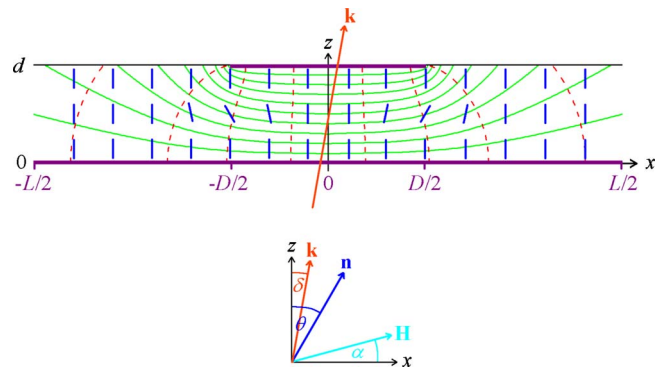


FIG. 5. (Color online) Geometry of the cell assumed in the calculations. The thick horizontal lines are the electrodes: infinite at $z=0$, finite ($-D/2 \leq x \leq D/2$) at $z=d$. The numerical calculations are done for the area $-L/2 \leq x \leq L/2$, $0 \leq z \leq d$. The thin solid lines are the equipotential lines; some lines of force for the electric field are shown dashed. The thick bars indicate the director orientation; θ is the director tilt angle. α is the misalignment angle of the magnetic field \mathbf{H} . The cell is illuminated by a monochromatic light in the direction \mathbf{k} deviating from the normal incidence by an angle δ .

IV. THEORETICAL MODEL

In this section we intend to calculate the director field in the constrained electrode geometry. The calculation is based on one basic concept of the continuum theory of nematics [1]: for stationary (reversible) deformations the free energy is minimized. In order to simplify the calculations we constrain ourself to a 2d geometry in the x - z plane, assuming that \mathbf{z} , \mathbf{E} , and \mathbf{H} lie all in this plane and there is no y dependence. This approximates the situation occurring in a vertical cross section of the cell at $y=0$ (i.e., through the center of the pixel).

The geometry considered is depicted in Fig. 5. The lower electrode at $z=0$ extends to infinity ($-\infty > x > \infty$) while the upper one, lying across at $z=d$, is finite ($-D/2 \leq x \leq D/2$). It is obvious that upon application of a voltage U to the electrode the electric field \mathbf{E} is the largest and is normal to the electrodes at $x=0$ (i.e., here $E_x=0$) while for $x \rightarrow \pm \infty$ one has $\mathbf{E} \rightarrow 0$. In general, due to the finite electrode size (the small aspect ratio D/d) the electric field is inhomogeneous in the cell and has an x component too: $\mathbf{E}(x,z) = (E_x(x,z), 0, E_z(x,z))$. It is convenient to introduce a single electric potential $\Phi(x,z) = Uu(x,z)$ which has the electric field as its gradient: $\mathbf{E} = -\nabla\Phi$. The magnetic field \mathbf{H} is assumed to be constant, making an angle α with the x axis: $\mathbf{H} = (H \cos \alpha, 0, H \sin \alpha)$. The director field is described by an angle $\theta(x,z)$ which gives the inclination of the director away from its initial homeotropic alignment: $\mathbf{n}(x,z) = (\sin \theta(x,z), 0, \cos \theta(x,z))$. The cell is illuminated by a monochromatic light of wavelength λ from the infinite electrode side; the direction of light propagation \mathbf{k} in general makes an angle δ with the cell normal (the z axis).

The calculations are made in two steps: first in Sec. IV A we compute $\mathbf{n}(\mathbf{r})$ for the case when a voltage is applied only, then in Sec. IV B we add the magnetic field too.

A. Director distortion in an inhomogeneous electric field

In this section we calculate the director field in the constrained electrode geometry in the absence of a magnetic field ($\mathbf{H}=0$).

The liquid crystal is assumed to be uncharged and insulating. If director gradients are present, the system gains an elastic free-energy density f_d which, in the present geometry, contains splay and bend terms only. The total free energy F is then composed of the volume integrals of f_d and that of the dielectric contribution f_e :

$$\begin{aligned} F &= \int [f_d + f_e] dV \\ &= \int \left[\frac{1}{2} K_1 (\text{div } \mathbf{n})^2 + \frac{1}{2} K_3 (\mathbf{n} \times \text{curl } \mathbf{n})^2 \right. \\ &\quad \left. - \frac{1}{2} \epsilon_0 \epsilon_{\perp} U^2 (\nabla u)^2 - \frac{1}{2} \epsilon_0 \epsilon_a U^2 (\mathbf{n} \nabla u)^2 \right] dV. \end{aligned} \quad (1)$$

Here K_1 and K_3 are the splay and bend elastic moduli, respectively. The dielectric anisotropy, $\epsilon_a = \epsilon_{\parallel} - \epsilon_{\perp}$, is the difference of dielectric permittivities measured along (ϵ_{\parallel}) and normal (ϵ_{\perp}) to the director \mathbf{n} . For the compound studied $\epsilon_a < 0$.

Due to the initial homeotropic alignment the boundary condition for the director is $\theta=0$ at both bounding surfaces (i.e., at $z=0$ and at $z=d$). The electric potentials at the boundaries are: $\Phi=0$ at the lower electrode (i.e., $u=0$ for $z=0$) as well as for $|x| \rightarrow \infty$ for any $z > 0$, while $\Phi=U$ at the upper electrode (i.e., $u=1$ for $z=d$ and $-D/2 \leq x \leq D/2$). It follows from the symmetry of the geometry that $u(x,z)$ is an even, $\theta(x,z)$ is an odd function of x (at the two edges of the electrode the electric field and hence the director tilts in the opposite direction); consequently $\theta=0$ at $x=0$ must fulfill.

In a typical cell of large aspect ratio at increasing U a bend Fredericksz transition would occur with a sharp threshold voltage U_F . In our case, however, the situation is modified due to the confined geometry; a deformation occurs near the electrode edges already for infinitesimally small U , while for $x \ll -D/2$ as well as for $x \gg D/2$ the homeotropic alignment prevails. The actual director field and electric potential should minimize the total free energy F in Eq. (1) with the boundary conditions mentioned above. This requirement leads to two coupled Euler-Lagrange equations; one for $\theta(x,z)$,

$$\begin{aligned} &(K_1 \cos^2 \theta + K_3 \sin^2 \theta) \frac{\partial^2 \theta}{\partial x^2} + (K_1 \sin^2 \theta + K_3 \cos^2 \theta) \frac{\partial^2 \theta}{\partial z^2} \\ &+ (K_3 - K_1) \sin \theta \cos \theta \left[\left(\frac{\partial \theta}{\partial x} \right)^2 - \left(\frac{\partial \theta}{\partial z} \right)^2 + 2 \frac{\partial^2 \theta}{\partial x \partial z} \right] \\ &+ (K_3 - K_1) (\cos^2 \theta - \sin^2 \theta) \frac{\partial \theta}{\partial x} \frac{\partial \theta}{\partial z} \\ &+ \epsilon_0 \epsilon_a U^2 \sin \theta \cos \theta \left[\left(\frac{\partial u}{\partial x} \right)^2 - \left(\frac{\partial u}{\partial z} \right)^2 \right] \\ &+ \epsilon_0 \epsilon_a U^2 (\cos^2 \theta - \sin^2 \theta) \frac{\partial u}{\partial x} \frac{\partial u}{\partial z} = 0, \end{aligned} \quad (2)$$

and one for $u(x,z)$,

$$\begin{aligned} &(\epsilon_{\perp} + \epsilon_a \sin^2 \theta) \frac{\partial^2 u}{\partial x^2} + (\epsilon_{\perp} + \epsilon_a \cos^2 \theta) \frac{\partial^2 u}{\partial z^2} \\ &+ 2 \epsilon_a \sin \theta \cos \theta \left(\frac{\partial^2 u}{\partial x \partial z} + \frac{\partial u}{\partial x} \frac{\partial \theta}{\partial z} - \frac{\partial u}{\partial z} \frac{\partial \theta}{\partial x} \right) \\ &+ \epsilon_a (\cos^2 \theta - \sin^2 \theta) \left(\frac{\partial u}{\partial z} \frac{\partial \theta}{\partial x} + \frac{\partial u}{\partial x} \frac{\partial \theta}{\partial z} \right) = 0. \end{aligned} \quad (3)$$

We note that Eq. (3) turns out to be equivalent to the Maxwell's equation $\text{div}(\epsilon \mathbf{E})=0$.

Unfortunately the resulting equations could not be solved analytically, so we had to obtain a numerical solution. Numerical calculations have been made on a two-dimensional grid covering the finite distance range $-L/2 \leq x \leq L/2$ and $0 \leq z \leq d$ with 417×21 points ($L=19.95d \approx 938 \mu\text{m}$, $D=311 \mu\text{m} \approx 6.6d$) using MATHEMATICA [17]. In the calculations the derivatives have been replaced by finite differences. The boundary condition for $|x| \rightarrow \infty$ could not be implemented on the finite grid. Instead, we assumed that the potential for $|x| > L/2$ at the upper substrate ($z=d$) is the same as it would be for an unperturbed homeotropic alignment. That ensures the stability of the solution.

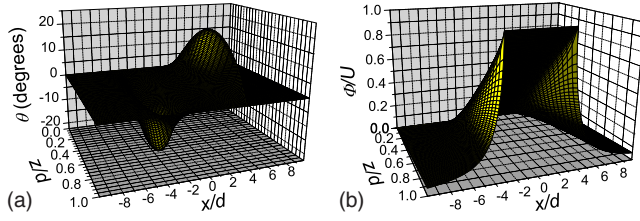


FIG. 6. (Color online) A three-dimensional plot of the calculated a; director tilt angle $\theta(x, z)$, and b; electric potential $\Phi(x, z)$ for the applied voltage $U=0.95U_F$ at $H=0$.

As an example of the numerical results in Fig. 6 we present three-dimensional plots of the calculated tilt angle $\theta(x, z)$ and potential $\Phi(x, z)$ for $U=0.95U_F$ at $H=0$. They reflect the required odd and even symmetry with respect to x . In Fig. 7 we compare the $\theta(x, d/2)$ profile in the middle of the cell for various applied voltages. It is seen that a distortion appears already much below the bulk Freedericksz threshold voltage U_F near the edge of the electrode ($x \approx \pm D/2$). This is the region where \mathbf{E} is not parallel to the initial director alignment, hence it bears some analogy to the simpler case of a homogeneous transition at tilted boundary conditions (initial director alignment is neither parallel nor perpendicular to the bounding surfaces but makes an angle β). In this latter case it has been proved that for $\beta \neq 0$, instead of the sharp Freedericksz transition at U_F , the distortion becomes thresholdless and θ_{\max} increases smoothly with U [2].

Figure 8 depicts the voltage dependence of the maximal tilt angle θ_{\max} . It has been found that the location z_{\max} where θ_{\max} occurs lies slightly above the middle of the cell (which is due to the asymmetric electrode configuration) and its x -position x_{\max} shifts slightly inside, away from the electrode edge with increasing U . For an illustration we plot in Fig. 9 the z dependence of the tilt angle at various x positions: at the electrode edge, and at a fixed distance from the edge inside and outside of the electrodes. It is also noticeable that the director tilt relaxes on a shorter length scale outside the electrodes than inside.

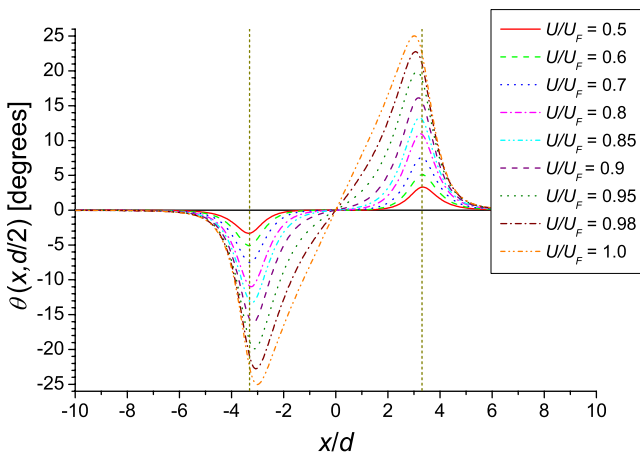


FIG. 7. (Color online) Calculated x -profile of the tilt angle $\theta(x, d/2)$ in the middle of the cell for various voltages U . The vertical dashed lines indicate the electrode edges.

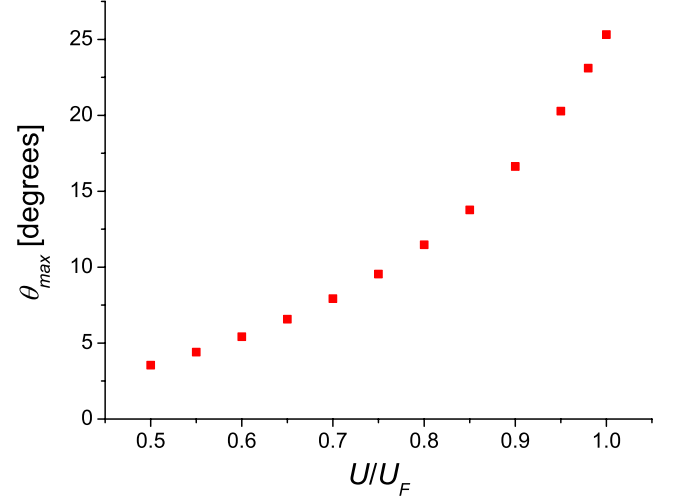


FIG. 8. (Color online) Calculated voltage dependence of the maximal tilt angle θ_{\max} .

Given the $\theta(x, z)$ dependence, one can easily calculate the optical phase difference $\Delta\Phi$ by integrating $n_{\text{eff}}(z) - n_o$ along z ,

$$\begin{aligned} \Delta\Phi &= \frac{2\pi}{\lambda} \int_0^d [n_{\text{eff}}(z) - n_o] dz \\ &= \frac{2\pi}{\lambda} \int_0^d \left[\frac{n_o}{\sqrt{1 - \frac{n_e^2 - n_o^2}{n_e^2} \sin^2 \vartheta}} - n_o \right] dz. \end{aligned} \quad (4)$$

Here $n_{\text{eff}}(z)$ is the effective refractive index for the extraordinary illumination depending on $\vartheta = \theta - \delta$ (the angle between the optical axis and the light propagation), while n_o is the ordinary, n_e is the extraordinary refractive index. $\Delta\Phi$ determines the transmitted light intensity detectable at crossed polarizers with a monochromatic illumination. In Figs. 10(a)–10(f) we exhibit the calculated x dependence of

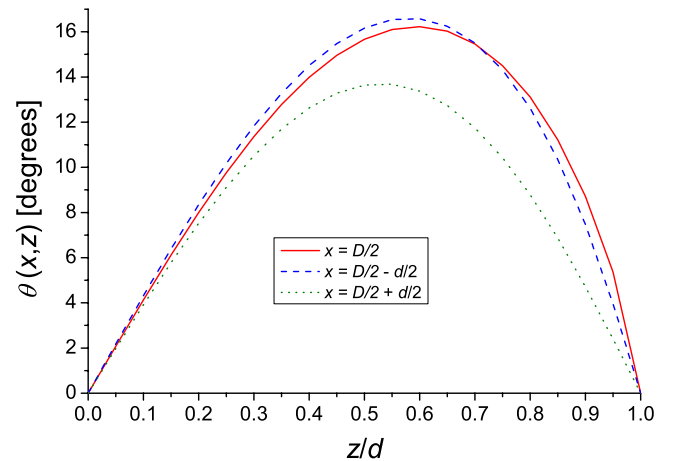


FIG. 9. (Color online) Calculated z -profile of the tilt angle $\theta(0, z)$ at the electrode edge, as well as inside and outside the pixel at $U=0.95U_F$.

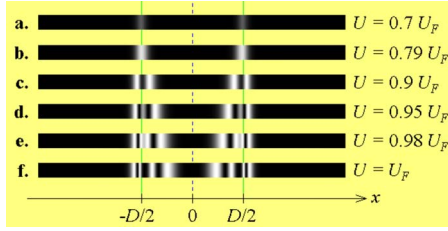


FIG. 10. (Color online) Reconstructed gray scale images at various voltages for the position dependence of the calculated transmitted intensity around the electrode edge at crossed polarizers. The vertical solid lines mark the location of the electrode edges; the dashed line is the center of the electrode.

the transmitted intensity for normal incidence ($\delta=0$) and $\lambda = 530$ nm in the form of gray scale images for different voltages, imitating what could be seen in the microscope.

The results of the simulation shown in Fig. 10 are in qualitative accordance with the images taken at white light illumination [Figs. 1(a)–1(d)]. For a quantitative comparison between simulations and experiments a set of images were taken of the same cell at monochromatic illumination by a green diode laser ($\lambda=530$ nm). In order to avoid the complications due to the fourfold symmetry of the images (field inhomogeneity and resulting deformation occurs at all four sides of the pixel), we focus onto a narrow horizontal section running along x through the center of the pixel where the effect of the other edges can mostly be neglected. Figure 11(a)–11(f) depicts such sections of the images. The agreement between Figs. 10 and 11 is very good up to $U = 0.98U_F$, i.e., in the range of relatively small deformations.

B. Inhomogeneous electric field with a superimposed homogeneous magnetic field

In this section we discuss the influence of a superposed homogeneous magnetic field \mathbf{H} on the director distortion. We assume that \mathbf{H} is mainly along x but allow for a slight misalignment characterized by an angle α (see Fig. 5) so that $\mathbf{H}=(H \cos \alpha, 0, H \sin \alpha)$. Due to the presence of the magnetic field there is an additional magnetic torque acting on \mathbf{n} which breaks the fourfold symmetry of the director field. At the electrode edges running normal to \mathbf{H} the electric and magnetic fields and the director are still coplanar, but at the

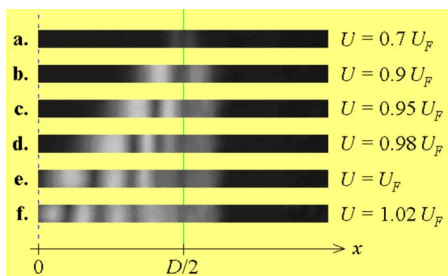


FIG. 11. (Color online) Position dependence of the measured transmitted intensity around the electrode edge at crossed polarizers in a type A cell. The vertical solid lines mark the location of the electrode edge; the dashed line is the center of the electrode.

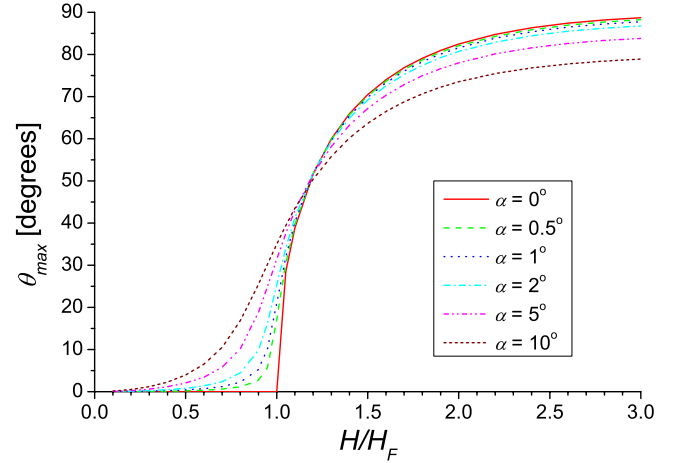


FIG. 12. (Color online) Calculated maximum distortion angle θ_{\max} of the deformation induced by an oblique magnetic field at $U=0$.

edges parallel to \mathbf{H} the electric field and hence the director gains a y component too. In the following we restrict ourselves to the simpler case of plane deformations. We follow the same route of calculations as above, just one has to take into account that the free-energy density of the system now contains a magnetic contribution, f_H , consequently F in Eq. (1) has to be supplemented by

$$F_H = \int f_H dV = \int -\frac{1}{2} \mu_0 \chi_a (\mathbf{nH})^2 dV, \quad (5)$$

where $\chi_a = \chi_{\parallel} - \chi_{\perp}$ is the anisotropy of the magnetic susceptibility, χ_{\parallel} and χ_{\perp} are the susceptibilities along and normal to the director, respectively (for the compound studied $\chi_a > 0$).

The direction of a magnetic field has an influence on the homogeneous Fredericksz transition, i.e., in cells of large aspect ratio. In Fig. 12 we plotted θ_{\max} as a function of H/H_F for different magnetic misalignment angles α (H_F is the threshold field for the magnetic Fredericksz transition). The curve $\alpha=0$ corresponds to the sharp Fredericksz transition. For oblique magnetic fields ($\alpha \neq 0$) the situation is the same as the case with tilted surface alignment, already mentioned before [2]: the deformation becomes thresholdless.

If a voltage U is on, for $\alpha=0$ the Fredericksz transition remains sharp; just the threshold voltage reduces with H . For $\alpha \neq 0$ the continuous character of deformation prevails, nevertheless the voltage necessary to induce a given θ_{\max} also reduces with H .

In our case of confined geometry the numerical determination of the director field can be done in the same way as for $H=0$, except that the sum of Eqs. (1) and (5) has to be minimized. As a consequence a magnetic term

$$\begin{aligned} & \mu_0 \mu_a H^2 \sin \theta \cos \theta (\cos^2 \alpha - \sin^2 \alpha) \\ & + \mu_0 \mu_a H^2 (\cos^2 \theta - \sin^2 \theta) \sin \alpha \cos \alpha \end{aligned} \quad (6)$$

should also be added to the left-hand side of Eq. (2).

The presence of the magnetic field does not break the symmetry if \mathbf{H} is parallel to the x axis ($\alpha=0$). A misalignment of \mathbf{H} ($\alpha \neq 0$) breaks, however, the left-right symmetry.

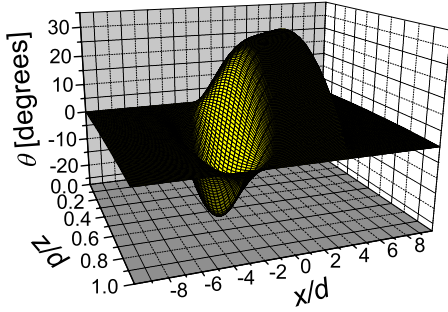


FIG. 13. (Color online) A three-dimensional plot of the calculated director tilt angle $\theta(x,z)$ for $U=0.79U_F$, $H=0.7H_F$, and $\alpha=0.5^\circ$.

This can be seen in the three-dimensional plot of $\theta(x,z)$ in Fig. 13 obtained for $U=0.79U_F$, $H=0.7H_F$ and $\alpha=0.5^\circ$. In Fig. 14 we compare the $\theta(x,d/2)$ profiles at $z/d=0.5$ for various misalignment angles α at $H=0.7H_F$ and $U=0.79U_F$. The location of the tilt inversion wall ($\theta=0$) shifts to the side by a distance s from the center. The bigger the misalignment angle, the bigger the shift, as demonstrated in Fig. 15. The shift of the inversion wall depends on the magnitude of \mathbf{H} too, as depicted in Fig. 16. For low H the shift s is small. It starts to increase strongly when H reaches the threshold magnetic field $H_{UF}=H_F(1-U^2/U_F^2)^{1/2}$ for the combined electric-magnetic Fredericksz transition. The calculations have shown that for higher magnetic fields (approaching H_F) the inversion wall can move out from the electrode area with an increasing slope of $s(H)$; finally, at a critical magnetic field close to H_F , the tilt inversion disappears.

Note the extreme sensitivity. A misalignment angle $|\alpha| < 0.5^\circ$ may produce already a shift of $|s| \approx 2d$.

The numerical results described above are in qualitative agreement with the experimental observations on type A cell shown in Figs. 3(a)–3(c) and 4 for $H \lesssim H_F$. One can notice, however, that the experimental slope of the $s(H)$ curve in Fig. 4 is only about 50% of the calculated one (Fig. 16). For high magnetic fields there is, moreover, even a qualitative difference. In contrast to the calculations, the experimental $s(H)$ curve in Fig. 4 behaves differently for high H : the inversion wall remained within the electrode area and did not disappear even for $H > H_F$.

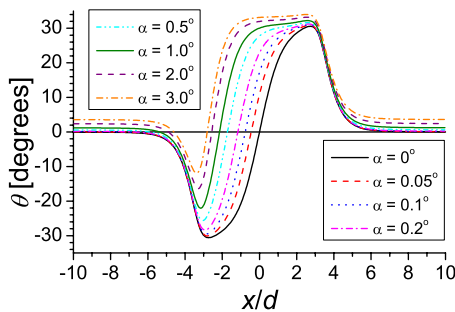


FIG. 14. (Color online) Calculated x -profile of the tilt angle $\theta(x,d/2)$ in the middle of the cell for various α angles at $H=0.7H_F$ and $U=0.79U_F$.

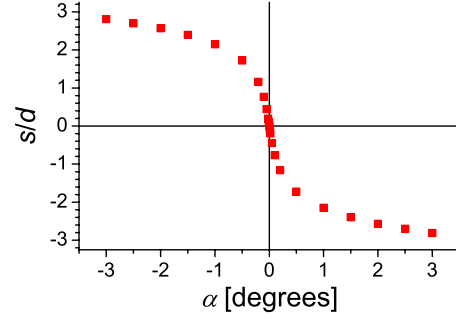


FIG. 15. (Color online) Calculated α dependence of the shift of the inversion wall at $H=0.7H_F$ and $U=0.79U_F$.

This deviation of the experimental findings from the predictions of the model can be attributed to the fact that the calculations have been done for a simplified geometry assuming no y dependence, while the electrodes of type A cell are actually finite (of size D , $N \approx 9$) also in the y direction. It can be seen in Fig. 3 that a strong director distortion does exist near those electrode edges running parallel to x . The elastic torques originating from this deformation zones—which are not taken into account in the presented calculations—may affect the position of the inversion wall. Formally this can be interpreted as if there were a restoring force acting on the inversion wall which hinders its displacement and prevents it from moving outside the electrode edges.

V. STRIP (1D) CONFINEMENT

In order to resolve the discrepancy mentioned above, experiments have also been performed on type B cells whose overlapping electrode area is a narrow strip extending along y to the cell edges. Type B cells have an aspect ratio of $N > 300$ in the y direction, thus approach the infinite cell assumption of the calculations much better.

A. Experimental observations on type B cells

The microphotographs in Figs. 17(a)–17(j) show an example how the electric-field induced deformation around the electrode edges of type B cell depend on the applied mag-

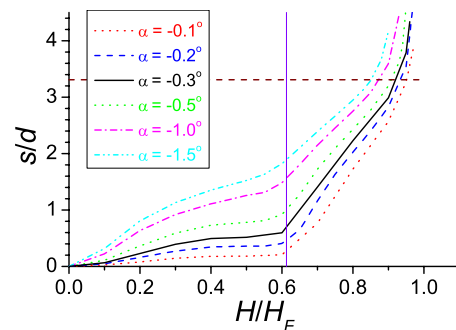


FIG. 16. (Color online) Calculated shift of the inversion wall versus H for various misalignment angles at $U=0.79U_F$. The dashed horizontal line indicates the position of the electrode edge; the vertical line marks the combined Fredericksz threshold H_{UF} .

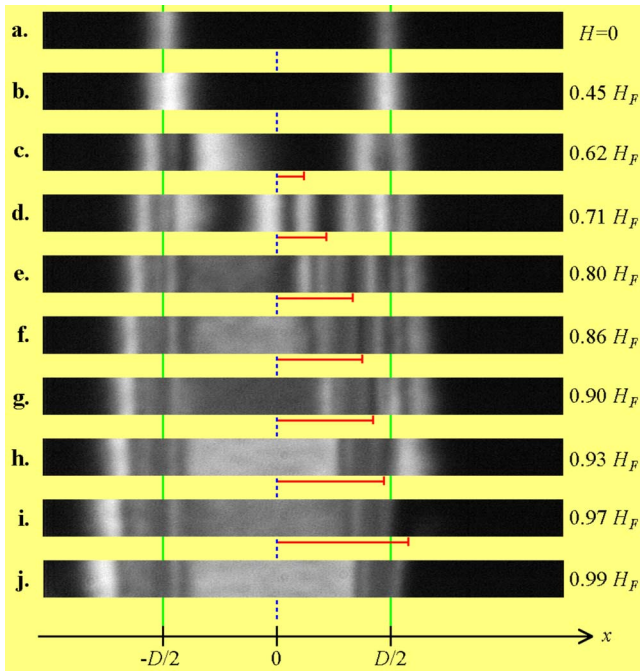


FIG. 17. (Color online) Microphotographs of the field induced deformation around an electrode strip in a type *B* cell at $U = 0.79U_F$ for various magnetic fields. The vertical solid lines mark the location of the electrode edges; the dotted line is the center of the electrode. The horizontal bars indicate the shift of the inversion wall.

netic field. These optical observations are in good qualitative agreement with the predictions of the calculations. They have proven that the deformation remains constrained to a region at the edges until the applied voltage U and magnetic field H reach the combined Fredericksz threshold ($H_{UF} = 0.61H_F$ for $U = 0.79U_F$). As a consequence there is a wide dark region in the center of the electrode [see Figs. 17(a) and 17(b)], so the position of the inversion wall cannot be precisely determined. Indeed, the calculations have shown that in this regime $|\partial\theta/\partial x| \approx 0$ at the location of $\theta = 0$. Above the threshold [i.e., in Figs. 17(c)–17(j)], however, $|\partial\theta/\partial x|$ is large; therefore the inversion wall appears as a narrow black line with a shift s from the center [indicated by horizontal bars in Fig. 17(c)–17(i)]. Figure 18 presents the magnetic field dependence of this shift for various applied voltages. It can immediately be seen that, in contrast to the case of type *A* cells shown in Fig. 4, for type *B* cell the slope of the $s(H)$ curve now increases with H . Moreover, the wall moves through the electrode edge and disappears completely for a critical $H \lesssim H_F$ [see the image at $H = 0.99H_F$ in Fig. 17(j)], just as the calculations predicted. This can be regarded as an indirect proof for the presence of a restoring force acting on the wall in 2d confined type *A* cell.

A quantitative comparison has also been attempted at $U = 0.79U_F$. Figure 18 shows besides experimental data the calculated shift for a quite small misalignment angle of $\alpha_{fit} = -0.3^\circ$ as a solid curve. It can be seen that this theoretical curve fits the measured data (solid squares) fairly well.

Unfortunately we do not have a direct tool to measure the actual misalignment angle α_0 (which is characteristic of the

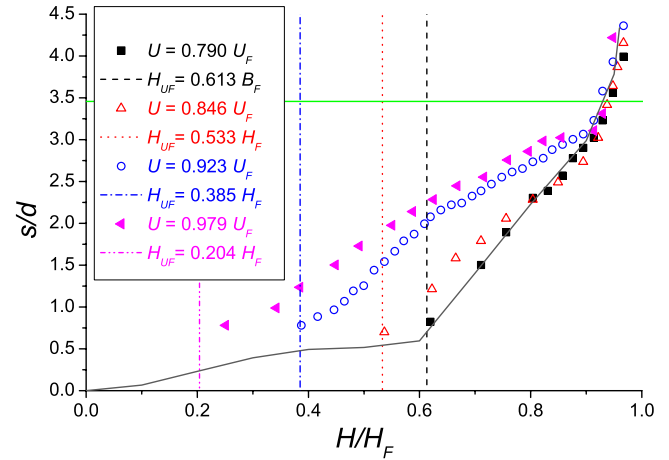


FIG. 18. (Color online) Shift s of the inversion wall from the center (in units of the sample thickness d) versus the magnetic field H (in units of the Fredericksz field H_F) at various applied voltages in a type *B* cell. The horizontal line marks the location of the electrode edge; the vertical lines show the threshold magnetic field of the combined electric-magnetic Fredericksz transition. The solid curve is the theoretical shift for $U = 0.79U_F$ and $\alpha_{fit} = -0.3^\circ$.

experimental setup) independently. We can, however, change this angle by rotating the cell in the magnetic field by a controlled angle $\Delta\alpha$ yielding $\alpha = \alpha_0 + \Delta\alpha$. One expects that when the misalignment is compensated by the rotation $\Delta\alpha = -\alpha_0$, the symmetry is restored and therefore the inversion wall should remain in the center of the electrode.

In Fig. 19 we present how does the cell rotation angle $\Delta\alpha$ affect the position of the inversion wall. It is seen that depending on the sign of $\Delta\alpha$ the shift of the wall can be larger as well as smaller than in case of $\Delta\alpha = 0$. Moreover, we can change the direction of the shift too. These measurements provide an indirect tool for the estimation of α_0 . In Fig. 20 the shift of the inversion wall is plotted versus $\Delta\alpha$ for two fixed magnetic fields. The data are well fitted by a second-order polynomial. The fit curves cross the x axis ($s = 0$) at $\Delta\alpha \approx 1.6^\circ$ implying that the initial misalignment angle is $\alpha_0 \approx -1.6^\circ$. This value is considerably bigger and seems to be more realistic than the one ($\approx -0.3^\circ$) which gave the best fit for the experimental data in Fig. 16.

We would like to note that a very small ($\approx -0.3^\circ$) misalignment angle could be realized by a cell rotation of $\Delta\alpha = +1.3^\circ$. In this case we have found that the inversion wall remains within the electrode area even for $H > H_F$ (see the open circles in Fig. 19). This observation disagrees with the predictions of the calculations in Sec. IV B shown in Fig. 16 and resembles the behavior found in 2d confined type *A* cell. This suggests that even in 1d confined type *B* cells there might exist a tiny restoring force hindering the motion of the wall (which is not taken into account in the calculations). Partly it might originate from the still finite (though large compared to d) size of type *B* cell, partly from pinning at surface defects outside the observed region of the cell. Such a restoring force could explain why the experimental shift of the inversion wall is less sensitive to the magnetic misalignment angle than the predictions of the calculations.

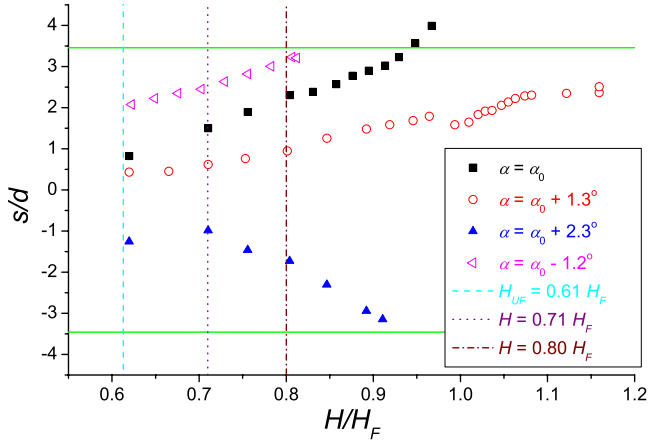


FIG. 19. (Color online) Shift s of the inversion wall from the center (in units of the sample thickness d) versus the magnetic field H (in units of the Fredericksz field H_F) at various cell rotation angles $\Delta\alpha = \alpha - \alpha_0$ at $U = 0.79U_F$ in a type B cell. The horizontal lines mark the location of the electrode edges; the vertical dashed line show the threshold magnetic field of the combined electromagnetic Fredericksz transition.

B. Influence of oblique light incidence

We have assumed so far for both the calculations (Fig. 10) and the evaluation of the experiments shown in Figs. 11 and 17 that the sample is observed at normal light incidence. This assumption allowed us to identify the extinction position (the darkest place in the image) with the position of the inversion wall. When the cell is rotated in the setup, not only α is varied but the light incidence angle δ is changing too. Therefore we have checked the influence of oblique light incidence on the observed textures.

At oblique light incidence, the optical phase difference developing in the cell depends on δ . As a consequence, if $\delta \neq 0$ the symmetry of the image seen in the microscope becomes broken already for $H=0$; namely, the intensity peaks originating from the deformed regions around the two electrode edges will have different heights. Such an asymmetry could be observed experimentally at $\Delta\alpha=0$ which renders a slight ($\delta_0 \approx 1^\circ$) obliqueness of the light incidence probable.

Another consequence of $\delta \neq 0$ is that the extinction position is shifted from the actual position of the inversion wall as it is illustrated in Fig. 21. It is seen that the dependence on δ is the strongest at low H where the tilt angles as well as $\partial\theta/\partial x$ are small. This is, however, the range where a precise comparison with the experiments cannot be performed. Whenever $\partial\theta/\partial x$ becomes already larger (in the $H > H_{UF}$ range), the extinction position becomes very weakly affected by the incidence angle. Therefore in that H range where the experiments were performed, the influence of the oblique incidence is practically negligible.

C. Influence of weak anchoring

In the calculations we assumed so far strong homeotropic anchoring, i.e., $\theta=0$, at the bounding substrates. This boundary condition does not hold, however, for a weak anchoring

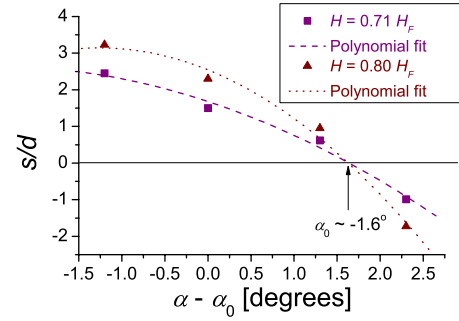


FIG. 20. (Color online) Shift s of the inversion wall from the center (in units of the sample thickness d) versus the cell rotation angles $\Delta\alpha = \alpha - \alpha_0$ at various magnetic fields H at $U = 0.79U_F$ in a type B cell. The lines correspond to a second-order polynomial fit.

where the director can tilt at the substrates too. Deviation from the (homeotropic) easy axis yields a surface free energy whose density is given as $f_s = \frac{1}{2}W \sin^2 \theta$ [18]. Here W characterizes the strength of anchoring; $W \rightarrow \infty$ corresponds to the strong anchoring case.

If weak anchoring is assumed the surface term

$$F_s = \int f_s dS|_{z=0} + \int f_s dS|_{z=d} = \int \frac{1}{2}W \sin^2 \theta dS|_{z=0} + \int \frac{1}{2}W \sin^2 \theta dS|_{z=d}, \quad (7)$$

should be added to the total free energy and should be involved into the minimization. Equations (2) and (3) will not be affected, but the boundary condition for the director should be replaced by

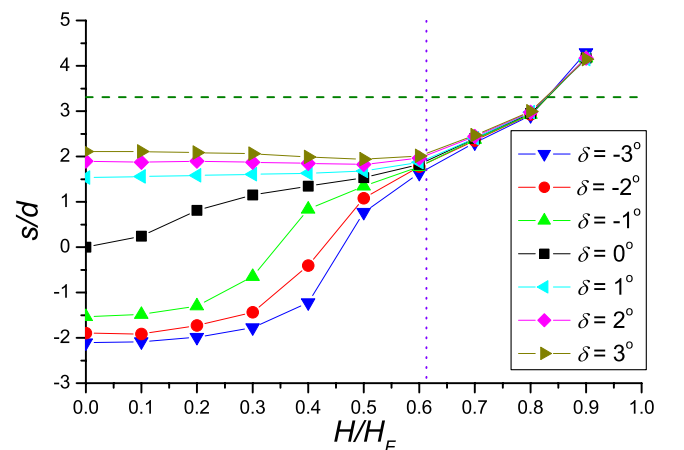


FIG. 21. (Color online) Shift s of the extinction position from the center (in units of the sample thickness d) versus the magnetic field H (in units of the Fredericksz field H_F) at $\alpha = -1.5^\circ$ and $U = 0.79U_F$ for various light incidence angles δ in a type B cell. The dashed horizontal line marks the location of the electrode edges; the vertical dotted line shows the threshold magnetic field H_{UF} of the combined electromagnetic Fredericksz transition.

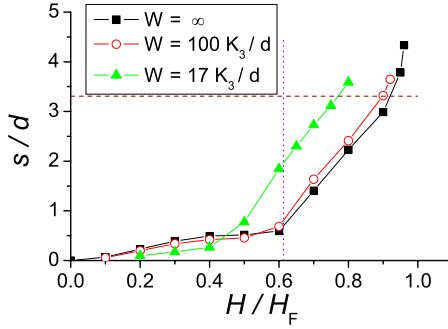


FIG. 22. (Color online) Calculated shift s of the inversion wall from the center (in units of the sample thickness d) versus the magnetic field H (in units of the Fredericksz field H_F) at $\alpha = -0.3^\circ$ and $U = 0.79U_F$ for strong as well as for weak anchoring of different strength. The dashed horizontal line marks the location of the electrode edges; the vertical dotted line shows the threshold magnetic field H_{UF} of the combined electric-magnetic Fredericksz transition.

$$(K_1 \sin^2 \theta + K_3 \cos^2 \theta) \frac{\partial \theta}{\partial z} + (K_3 - K_1) \sin \theta \cos \theta \frac{\partial \theta}{\partial x} \pm W \sin \theta \cos \theta = 0 \quad (8)$$

where the minus sign applies for the $z=0$ substrate, while the plus sign should be taken for $z=d$ [19].

The anchoring strength affects the Fredericksz thresholds too; actually lowers them. With straightforward calculation one obtains that the Fredericksz threshold voltage U_{Fw} at weak anchoring is related to the threshold voltage U_F at strong anchoring by

$$U_{Fw} = \left(1 - \frac{2\xi_0}{\pi}\right) U_F \quad \text{with} \quad \sin^2 \xi_0 = \frac{\left(\pi \frac{U_{Fw}}{U_F}\right)^2}{\left(\frac{Wd}{K_3}\right)^2 + \left(\pi \frac{U_{Fw}}{U_F}\right)^2}. \quad (9)$$

A similar prefactor applies for the magnetic threshold field too.

For our cell the experimental value of the bulk Fredericksz threshold voltage is about 91% of the theoretical value (calculated from the material parameter set [16]). If this difference is fully attributed to the effect of the finite anchoring strength (which may be an overestimation), one obtains $W \approx 17K_3/d \approx 4.6 \times 10^{-6} \text{ J m}^{-2}$, which is of the usual order of magnitude [20].

Simulations for our confined geometry have shown that weakening the anchoring (lowering W) increases the distortion angle, as expected. The influence of the finite anchoring strength on the displacement of the inversion wall in magnetic field is demonstrated in Fig. 22, where the field dependence of the shift of the inversion wall at various anchoring strengths is compared with that calculated for strong anchoring. It is seen that at small magnetic fields ($H < H_{UF}$) the shift of the wall is slightly smaller for weak anchoring, however, for higher magnetic fields ($H > H_{UF}$, which is relevant to compare with measurements) lowering the anchoring

strength increases the displacement of the inversion wall from the center. In addition, at weak anchoring the wall can move out of the electrode area already at lower magnetic fields.

VI. SUMMARY

In this work we have studied the deformation of a homeotropic nematic liquid crystal in a confined geometry (around the electrode edges) in superposed electric and magnetic fields. Both 2d (square electrodes) and 1d (strip electrodes) confinements have been tested experimentally. It has been found that at increasing voltages director distortion emerges around the electrode edges leading to the appearance of defects in the center of the cell, while an additional magnetic field shifts the defect from the center. The qualitative explanation of the observed phenomena relies on the presence of inhomogeneous electric fields superposed with a homogeneous, though slightly misaligned magnetic field. This idea has been supported by numerical simulations based on the continuum theory performed for the 1d geometry. Simulations could give an account of most experimental features, though yielded a larger sensitivity of the defect's shift on the magnetic misalignment angle than found experimentally by cell rotation measurements.

Most simulations have been performed for idealized conditions; namely, assuming electrode strips of infinite length, strong anchoring and no pretilt at the bounding surfaces, normal light incidence, insulating liquid crystal with no flexoelectric interaction. There is no reason to assume the presence of a (uniform) pretilt in the sample considering the lack of alignment coating. The influence of oblique light incidence and weak alignment has been explicitly checked by simulations yielding that none of these factors can reduce the sensitivity to the misalignment considerably.

As there is a splay-bend deformation in our geometry, flexoelectric polarization [1] may arise around the electrode edges which interacts with the electric field and thus may affect the resulting director field. Flexoelectricity has, however, been neglected during the simulations; not only because of the lack of knowledge of the precise values of the flexoelectric coefficients, but also to allow comparison with our measurements at $f=1 \text{ kHz}$. This frequency is much exceeding the inverse director relaxation time and therefore flexoelectricity and charge screening effects are expected to play much less role. In addition, the exposition time of our camera was much longer than the period of the ac voltage, hence any remaining modulation due to the linear flexoelectric interaction is averaged out in the recorded images. Therefore neglecting flexoelectricity is not expected to be the reason for the high theoretical sensitivity to magnetic misalignment.

The lower experimental sensitivity to the field misalignment can be resolved by assuming a restoring force which hinders the shift of the inversion wall. Such a force might originate on the one hand in director pinning at surface defect, on the other hand it should surely occur due to the deformation at the electrode edges parallel to x in case of 2d confinement (see Fig. 3), but might also be present (though

with considerably smaller magnitude due to the finite (though large) size of the electrode strip in the case of 1d confinement. Calculation of its influence would require an extension of the model to 3d deformations which may be a task for the future.

ACKNOWLEDGMENT

Financial support by the Hungarian Research Fund Grants No. OTKA K61075 and No. K81250 is gratefully acknowledged.

-
- [1] P. G. de Gennes and J. Prost, *The Physics of Liquid Crystals* (Oxford Science Publications, New York, 2001).
- [2] L. M. Blinov and V. G. Chigrinov, *Electrooptic Effects in Liquid Crystal Materials* (Springer, New York, 1996).
- [3] *Pattern Formation in Liquid Crystals*, edited by Á. Buka and L. Kramer (Springer-Verlag, New York, 1996).
- [4] T. Nose and S. Sato, *Liq. Cryst.* **5**, 1425 (1989).
- [5] G. Haas, H. Wöhler, M. W. Fritsch, and D. A. Mlynski, *Mol. Cryst. Liq. Cryst.* **198**, 15 (1991).
- [6] V. G. Chigrinov, I. N. Kompanets, and A. A. Vasilev, *Mol. Cryst. Liq. Cryst.* **55**, 193 (1979).
- [7] V. G. Chigrinov, *Mol. Cryst. Liq. Cryst.* **179**, 71 (1990).
- [8] C.-D. Wang and G.-C. Yang, *Acta Phys. Sin. (Overseas Ed.)* **6**, 422 (1997).
- [9] Ch. Cramer, U. Kühnau, H. Schmiedel, and R. Stannarius, *Mol. Cryst. Liq. Cryst.* **257**, 99 (1994).
- [10] H. Schmiedel, Ch. Cramer, R. Stannarius, K. Eidner, and M. Grigutsch, *Liq. Cryst.* **14**, 1935 (1993).
- [11] M. Hartung, *Abnormale Rollen in Elektrokonvektion von Flüssigkristallen mit subkritischer Bifurkation* (Diplomarbeit, Universität Bayreuth, Bayreuth, Germany, 2003).
- [12] T. Mullin, S. J. Tavener, and G. I. Blake, *J. Non-Newtonian Fluid Mech.* **119**, 61 (2004).
- [13] S. Rudroff, H. Zhao, L. Kramer, and I. Rehberg, *Phys. Rev. Lett.* **81**, 4144 (1998).
- [14] Á. Buka, P. Tóth, N. Éber, and L. Kramer, *Phys. Rep.* **337**, 157 (2000).
- [15] Y. Koike and K. Okamoto, *Fujitsu Sci. Tech. J.* **35**, 221 (1999).
- [16] M. Treiber, N. Éber, Á. Buka, and L. Kramer, *J. Phys. II* **7**, 649 (1997).
- [17] The calculations presented in the paper have been checked for some selected parameters by simulations using a much higher resolution irregular triangular grid in COMSOL MULTIPHYSICS. No significant difference could be observed between the results obtained by the different techniques.
- [18] A. Rapini and M. Papoular, *J. Phys. Colloq.* **30**, C4-54–C4-56 (1969).
- [19] G. Napoli, *J. Phys. A* **39**, 11 (2006).
- [20] Ch.-J. Yu J.-H. Park, and S.-D. Lee, *Appl. Surf. Sci.* **238**, 385 (2004).